We are IntechOpen, the world's leading publisher of Open Access books
Built by scientists, for scientists

6,000
Open access books available

148,000
International authors and editors

185M
Downloads

Our authors are among the

154
Countries delivered to

TOP 1%
most cited scientists

12.2%
Contributors from top 500 universities

CLARIVATE ANALYTICS
BOOK CITATION INDEX
INDEXED

WEB OF SCIENCE™

Selection of our books indexed in the Book Citation Index
in Web of Science™ Core Collection (BKCI)

Interested in publishing with us?
Contact book.department@intechopen.com

Numbers displayed above are based on latest data collected.
For more information visit www.intechopen.com

Chapter

Synthesis of Pt-Mo/WMCNTs Nanostructures Reduced by the Green Chemical Route and Its Electrocatalytic Activity in the ORR

Esther Torres-Santillan, Selene Capula-Colindres,
Gerardo Teran, Carmen M. Reza-San German,
Miriam Estrada Flores and Oscar Guadalupe Rojas Valencia

Abstract

Platinum (Pt) and molybdenum (Mo) nanoparticles were supported on multiwall carbon nanotubes (MWCNTs) by a green chemical route. Different relations of Pt:Mo (10:0, 8:2, 5:5, 2:8, and 0:10, respectively) in weight percent were compared to their electrocatalytic activity in the oxygen reduction reaction (ORR) in an acid medium. The morphologies and the structure were analyzed by X-ray diffraction (XRD), scanning electron microscopy (SEM), and transmission electron microscopy (TEM). The rotary disc electrode (RDE) and linear voltammetry (LV) techniques were employed to observe the electron transfer and mass transport phenomena. The surface activation of the samples was conducted by cyclic voltammetry (CV) technique According to the TEM analysis. The TEM analysis, shows that Mo and Pt nanoparticles have a good dispersion on the tubular carbon support, with sizes between 3.94 and 10.97 nm. All Pt-containing ratios had exhibited a first-order transfer in the ORR without inhibition of the reaction. Molybdenum is a reducing agent (oxyphilic metal) that benefits the adsorption of oxygenated species. The Pt:Mo 8:2 wt.% ratio presents the maximum benefits in the kinetic parameters. The Mo_{10}/MWCNTs nanostructure inhibits the ORR due to the strong bonds it presents with oxygen. Molybdenum at low concentrations with platinum is conducive to oxygen molecule adsorption-desorption by increasing the ORR's electroactivity.

Keywords: molybdenum, platinum, oxygen reduction, MWCNTs, oxyphilic metal

1. Introduction

It is widely recognized in the field of electrochemistry that there are many important electrochemical reactions. Some cases are the oxygen reduction reaction

(ORR) and the hydrogen oxidation reaction (HOR). These reactions can be set in the proton exchange membrane fuel cells (PEMFCs) for the generation and storage of clean energy [1–3]. ORR takes place at the cathode of the PEMFCs where it is highly sensitive to the surface of the electrode and the presence of adsorbed oxygenated species. As pointed out above, this is due to the stability of the oxygen molecule and the double bond, requiring a greater potential (1.23 V) to take place a reduction [4–7]. To obtain a high conversion at ORR, the catalyst Pt/C has been used for its high catalytic activity and chemical stability [8–10]. The previous properties of Pt induce a direct transfer of four electrons to form water, therefore presenting a first-order transfer. However, several investigations have reported a kinetic inhibition in the ORR by the adsorption of different pollutants (CO, SOx, and NOx) on the electrode surface, causing poisoning of the Pt catalysts [11, 12]. The commercial carbon support is a crucial factor in the deactivation of PEMFCs by its corrosion at high potentials (>0.5 V) [12–14]. Due to the high cost of Pt, various catalysts have been proposed, such as oxides [15, 16], carbides [17, 18], Pd [19, 20], binary, tri-metallic alloys (Pt, Ru, Pd, or Ir) [21–25], non-precious metals, and supercycles (porphyrins or phthalocyanines) [26, 27]. Despite the efforts made, it is difficult to replace the Pt as a catalyst in the cathode for the PEMFCs. It is because the catalyst should have good electrocatalytic activity and resistance for both CO and acid [28–30]. Furthermore, it must present efficient adsorption and desorption of oxygenated species in the interface electrode/electrolyte. If the adsorption–desorption of oxygenated species is deficient in the OER, then there will not be a good electronic transfer, or desorption of species when the ORR is carried out.

Nepel et al. [31] and Mukerjee et al. [32] have found that molybdenum is a metal that allows greater tolerance to CO. Besides, Mo is used by biological systems mainly for its oxidative and reducing properties [33]. Additionally, it is used as a catalyst for desulfurization and denitrogenating processes in the petrochemical industry [34]. Molybdenum is an element with a "d" band characteristic in its electronic configuration. It can have different crystalline phases and superficial and electronic properties according to its geometric arrangements. It can be polymerized to form anionic poly-molybdates (Mo^{VI}), which present reactions of transfer of oxygen atoms to potential chemicals, less than 0.1 V. According to Pérez et al. [35] and Nikolaychuk et al. [36], these polymolybdates undergo redox reactions to potentials higher than 0.2 V. The molybdenum is one of the few affordable elements that act as a "source" of electrons and can transfer oxygen atoms to low potential values. These properties, electronics, and transference (adsorption–desorption) of oxygen atoms have not been widely investigated for the ORR in the acid medium [33, 37]. Another alternative of research to improving the electrocatalytic activity of the ORR is the study of various supports. Recent works performed by Hussain et al. [38] and Huang et al. [39] indicated that carbon in its allotropic tubular form has a greater specific area and chemical stability in the ORR than conventional commercial carbon. The CNTs (carbon nanotubes) have considerable advantages, including greater resistance to potentials greater than 0.5 V without generating CO. Efficient dispersion of the nanoparticles on the support, which generate a high activity, in comparison to the conventional carbon support [40–42].

This study aims to synthesize Pt-Mo/MWCNTs nanostructures by the wet impregnation method, produce different Pt-Mo loads in the nanostructures, achieve an elevated dispersion of the nanoparticles on the support (MWCNTs), conduct

an electrochemical work to determine the effect of the molybdenum content in the electroactivity for the ORR, examine the importance of the content of an oxyphilic metal such as molybdenum in a bimetallic catalyst for the ORR in an acidic medium, determine the best ratio of Pt-Mo to achieve the first-order mechanism without inhibition of the reaction, and finally, obtain the kinetics parameters and the type of electronic transference mechanism that takes place.

2. Experimental section

2.1 Synthesis of nanostructures

Commercially available MWCNTs synthesized by the method CVD (chemical vapor deposition, ≥97% purity) were used as support and acquired from Sigma-Aldrich. Commercial MWCNTs were pretreated by warming to reflux in a mixture of HNO_3 and H_2SO_4 (8 M) at 80°C for 3 h [43]. MWCNTs were thoroughly filtered and washed with deionized water, with subsequent drying on the stove for 24 h at 60°C. For the nanoparticles impregnation on the support, bis(acetylacetonate)dioxo-molybdenum [$MoO_2(CH_3COCH_2COCH_2)_2$, Sigma-Aldrich, 98% purity] and platinum acetylacetonate [$Pt(CH_3-COCHCO-CH_3)_2$, Sigma-Aldrich, 97% purity] were used as precursors. Different Pt-Mo relations were implemented to obtain 10 wt.% (10:0, 8:2, 5:5, 2:8, and 0:10, respectively). Pretreated MWCNTs support was set in a balloon flask with isopropanol and agitation of 900 rpm at 70°C for 1 h. Subsequently, the mixture of the precursors previously dissolved in isopropanol was added dropwise and stirred for 2 h until complete. A solution of eucalyptus extract (5 g/100 ml water) was added as a green reduction agent, and the mixture was stabilized with ethylene-glycol (EG). The solids were filtered, and the mixture was washed with deionized water. Eventually, the solids were dried at a temperature of 60°C. Consequently, the solids were placed in a quartz tube with a glass membrane and kept in an oven at 300°C for 30 minutes. At this step, a minimum flow of H2 for complete reduction.

2.2 Structural and morphological characterization

The crystalline structure and particle size were analyzed by X-ray diffraction (XRD) using an X-ray diffraction equipment, Siemens D5000 with a Cu-K α1 monochromatic radiation (λ = 1.548 A), operating at 40 kV and 40 mA at 10–90° 2θ range and a scan rate of 2°/s. The morphologies and chemical composition of the samples were determined by scanning electron microscopy (SEM) coupled with energy-dispersive spectroscopy (EDS) using a detector SEM-JEOL 6300. Transmission electron microscopy measurements were used to investigate the morphology, size, and dispersion of metal nanoparticles on MWCNTs. In this research, a Titan (FEI) microscope, operating at an accelerating voltage of 200 kV, was employed. The samples were prepared and deposited on the standard TEM sample grid covered with holey carbon film.

2.3 Electrochemical system

Oxygen reduction reaction activity was measured in a standard three-electrode system comprising a working electrode (RDE0008 commercial electrode), a

hydrogen reference electrode (ET070 Hydroflex), and a counter electrode (Pt coil). An electrolyte of 0.5 M H_2SO_4 was used. To prepare the catalyst ink, 1 mg of Pt-Mo/ MWCNTs powder was weighed to which 75 µL of ethanol was added to disperse it. Afterward, 8 µL of a mixture of Nafion® liquid and ethanol (5 wt.%) were added as an adherent to the electrode and 15 µL of water. An ultrasonic bath was employed for 20 minutes to homogenize the catalyst ink. A 16 µL aliquot of the catalyst ink was then pipetted onto the glassy carbon disk of 0.19 cm^2 of the area. By applying the cyclic voltammetry technique with a scanning speed of 50 mV s^{-1}, the activation of the electrode is recorded between 0 and 1.2 V during 100 cycles in a solution of 0.5 M H_2SO_4 saturated with argon.

To obtain kinetic parameters, the technique of linear voltammetry in a range of potential from open circuit to 0 V in a cathode ray with a speed of 5 mVs^{-1} was collected at 100, 200, 400, 900, 1600 rpm on the disk in the oxygen-saturated electrolyte. The experimentation was performed at 25°C and an atmospheric pressure of 585 mmHg. A potentiostat-galvanostat Autolab PGSTAT302 was employed, and all reported voltages were referred to as the normal hydrogen potential (NHE).

3. Results and discussion

3.1 Morphological characterization of Pt-Mo/MWCNTs nanostructures

Figure 1(a)-(f) shows the XRD patterns of the MWCNTs support and Pt-Mo/ MWCNTs nanostructures with different nominal ratios of Pt-Mo (0:0, 0:10, 2:8, 5:5, 8:2, and 10:0) wt.%. The large reflections at 2θ = 39.7°, 46.2°, 67.6°, and 81.4° are associated with the face-centered-cubic (*fcc*) Pt crystal structure corresponding to the (111), (200), (220), and (311) planes, respectively, according to (PDF 04-0802). The reflection at 2θ = 26.2° corresponds to a crystal plane (002) of the hexagonal graphite structure (PDF 056-0159). Reflections of Pt in Pt-Mo/MWCNTs nanostructures shift slightly to higher angles compared with those of Pt in Pt/MWCNTs, which is evidence of lattice contraction caused by alloying Pt-Mo. The extent of lattice contraction increases to increase Mo content, in Pt-Mo/MWCNTs nanostructures, as shown by the lattice listed in **Table 1**. Previous research shows that lattice contraction is an indication of partial substitution of Mo for Pt in the Pt lattice [44–46]. The particle sizes of Pt were calculated with Scherrer equation, on (200) for reflection are not affected by MWCNTs support. Pt particle size was between 3.78 and 6.18 nm. The intensity of the Pt reflection gradually increases with a higher Pt content and broadens further in the XRD patterns indicating a smaller particle size. This behavior can be attributed to the high mobility of metal nanoparticles on carbon nanotube surfaces due to weak interaction between metal and support [47].

Figure 2(a-f) shows TEM micrographs of Mo_{10}/MWCNTs, Pt_2Mo_8/MWCNTs, Pt_5Mo_5/MWCNTs, Pt_8Mo_2/MWCNTs, and Pt_{10}/MWCNTs nanostructures. The images reveal nanoparticles evenly distributed on the MWCNTs surface. The shape of Mo nanoparticles is elongated with an average particle size of 10.97 nm (**Figure 2a**). All the nanostructures with Pt exhibited a circular shape with an average size for the nanoparticles between 3.94 and 6.96 nm. (**Figure 2b-d, f**). The particle dimensions measured by TEM are consistent with the average size determined from the corresponding XRD patterns. In the Pt_8Mo_2/MWCNTs nanostructure, the size in TEM images is slightly larger. High-resolution transmission electron microscopy (HR-TEM) images of the Pt_8Mo_2/MWCNTs revealed their crystalline nature (Inset **Figure 2e**).
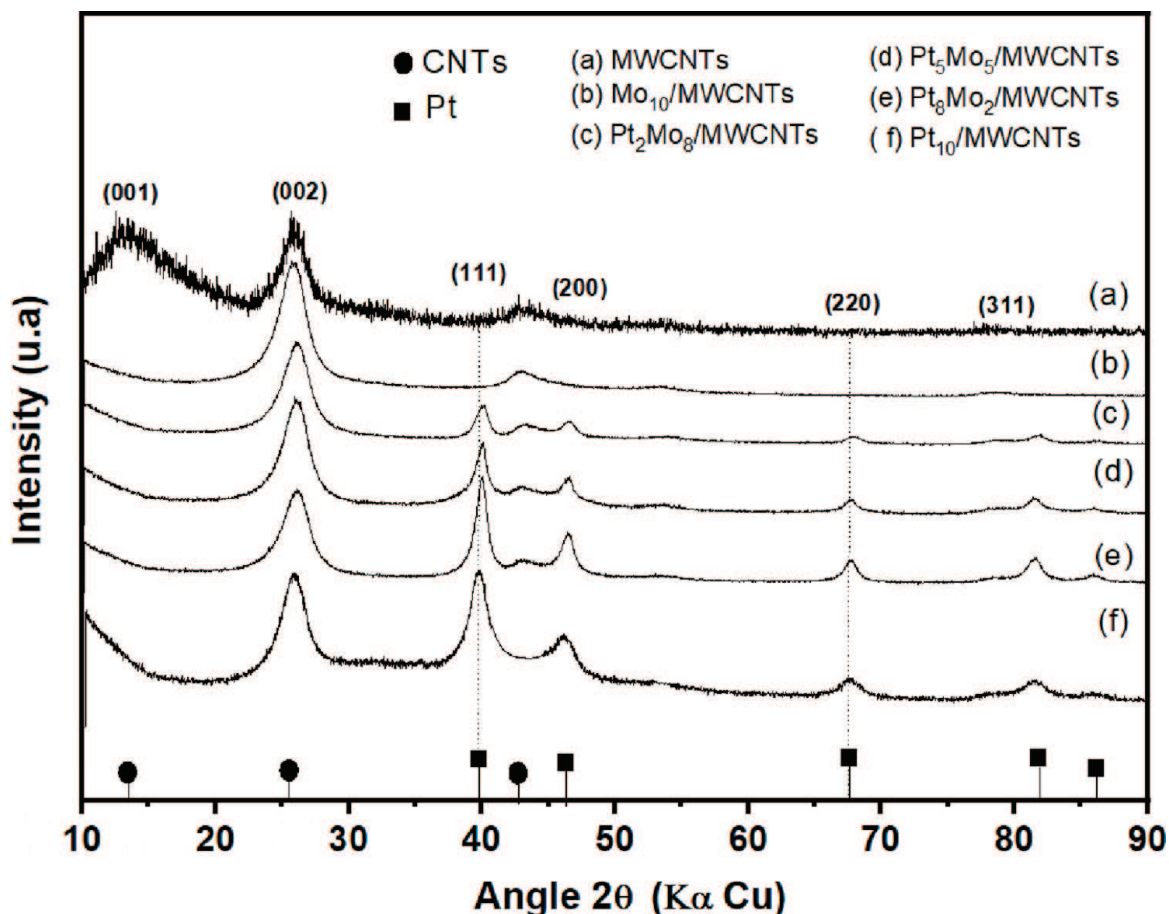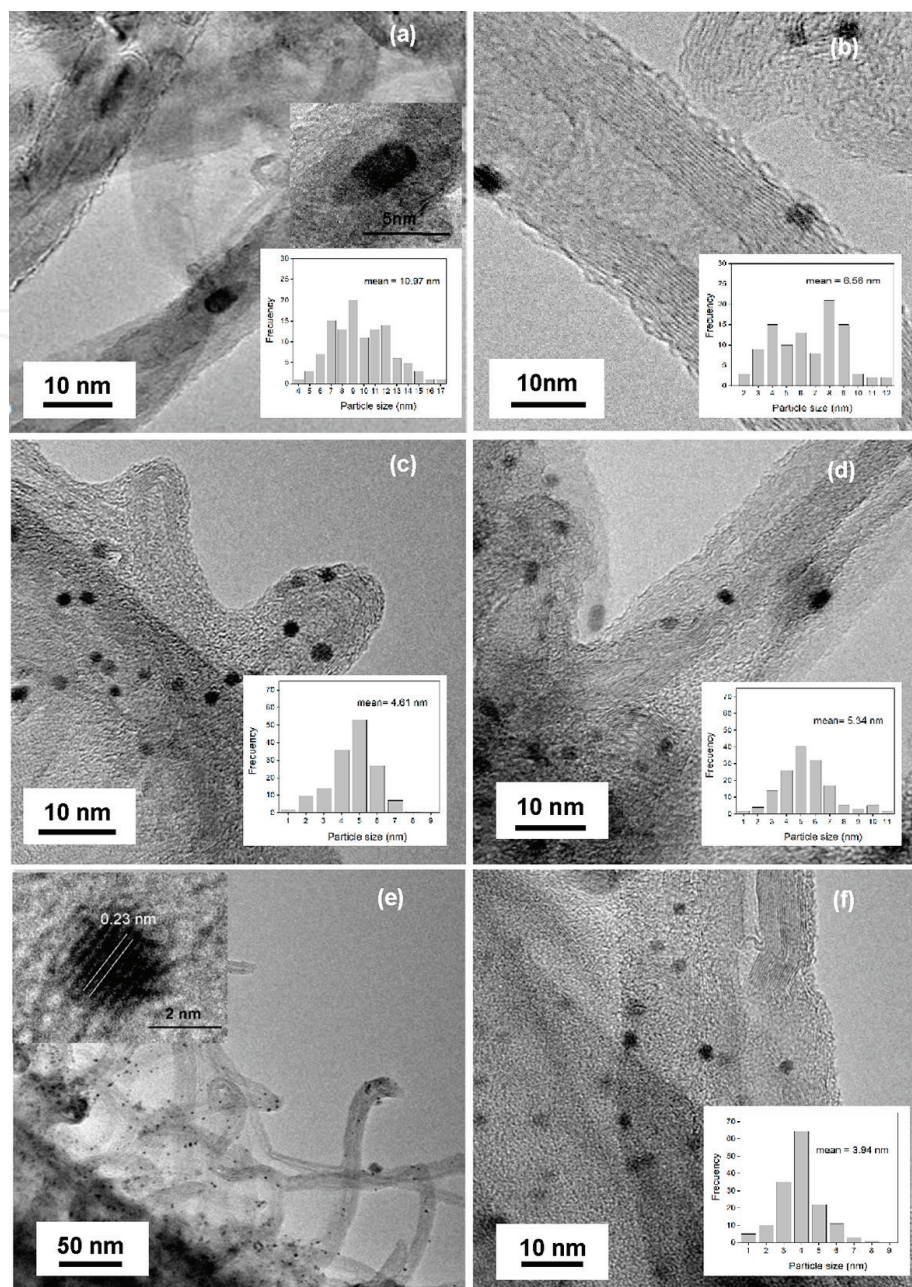
Figure 1.
XRD patterns of MWCNTs and Pt-Mo/MWCNTs nanostructures.

Nanostructures	Pt:Mo atomic Ratio		Lattice Parameter	Particle size by XRD
	Nominal	EDS	Å	(nm)
Mo10/MWCNT	100	83	—	—
Pt2-Mo8/MWCNTs	20:80	24:76	3.805	6.18
Pt5-Mo5/MWCNTs	50:50	53:46	3.908	4.61
Pt8-Mo2/MWCNTs	80:20	83:17	3.913	5.54
Pt10/MWCNTs	100	92	3.985	3.78

Table 1.
Data obtained from XRD-EDS analysis.

The spacing between adjacent lattice planes is around 0.23 nm, corresponding to (111) plane of *fcc* structure Pt [44]. For the inset (HR-TEM) image of the Mo_{10}/MWCNTs nanostructure, there is no d-spacing lattice of metallic Mo, Mo oxide, or Mo carbide structure.

Images of Pt_{10}/MWCNTs and Pt_5Mo_5/MWCNTs obtained by SEM are displayed in **Figure 3(a-b)**. The tubular structure of MWCNTs support can be observed in these images. The average diameter of an MWCNT is within 20–30 nm. EDS spectrum shows the presence of Mo and Pt in the structure (**Figure 3c-d**). The elemental chemical composition of Mo and Pt is also provided in **Table 1**. The atomic ratios of Pt
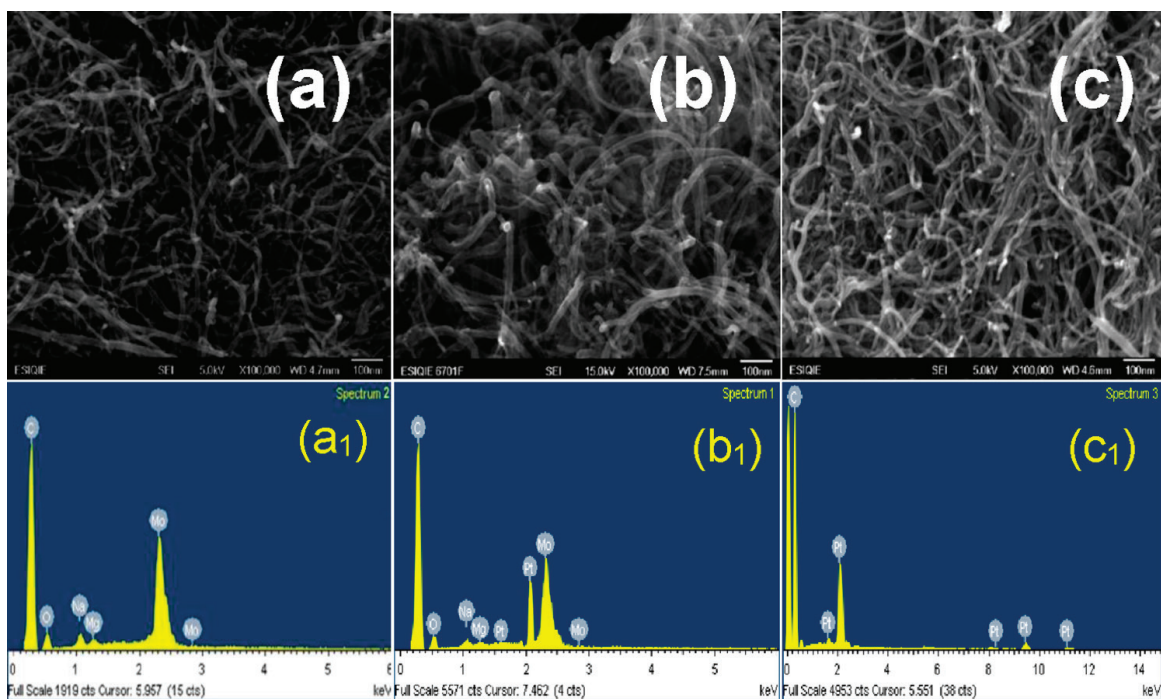
Figure 2.
TEM micrographs (a) Mo10/MWCNTs, (b) Pt2Mo8/MWCNTs, (c) Pt5Mo5/MWCNTs, (d-e) Pt8Mo2/ MWCNTs, and (f) Pt10/MWCNTs.

and Mo are close to nominal composition, suggesting the effective reduction of Pt and Mo by the impregnation method used.

3.2 Electrochemistry characterization

Cyclic voltammograms of Mo_{10}/MWCNTs, Pt_2Mo_8/MWCNTs, Pt_5Mo_5/MWCNTs, Pt_8Mo_2/MWCNTs, and Pt_{10}/MWCNTs nanostructures are graphically presented in **Figure 4**. The samples with 5, 8, and 10 wt.% of Pt manifested a typical behavior of an electrode with this material in an acid medium [9, 40]. The area associated with the adsorption–desorption of protons is presented in the region from 0 to 0.30 V/ NHE for all nanostructures. The samples containing Pt_{10} and Pt_2Mo_8 present a peak more intense in the previous zone, it is indicating greater performance in the

Figure 3.
SEM-EDS imaging of (a-a1) Mo10/MWCNTs and (b-b1) Pt5Mo5/MWCNTs and (c-c1) Pt10/MWCNTs samples.
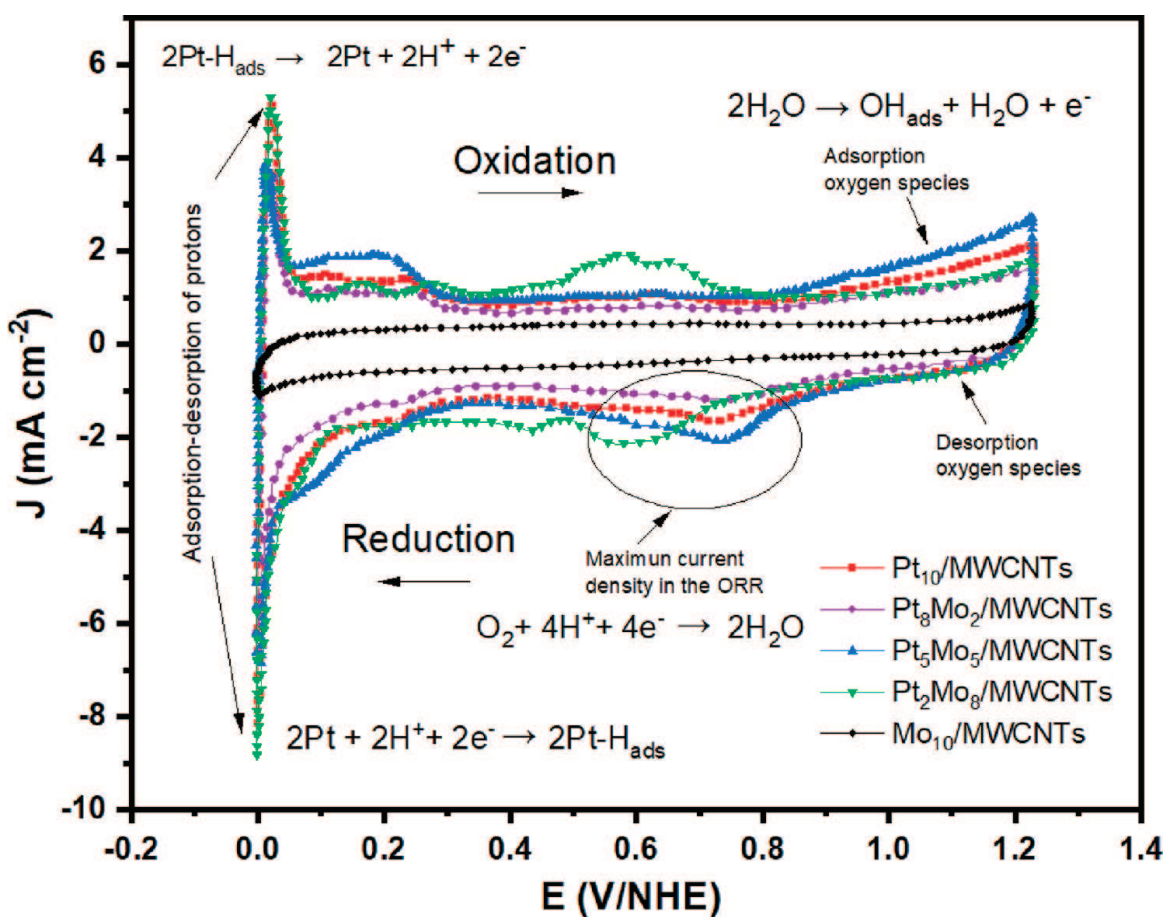

Figure 4.
Cyclic voltammetry Pt-Mo/MWCNTs nanostructures (sweep speed 50 mVs⁻¹, 25°C, last cycle).

hydrogen evolution reaction and the hydrogen oxidation reaction (HOR). According to Grgur et al. [48], the mechanism for interaction of oxygenated species with bimetallic surfaces must contain a metal capable of dissociating hydrogen and a metal that forms strong M − O bonds. The high activity of Pt for the hydrogen oxidation reaction is attributed to its ability to dissociate hydrogen as presented in Eq. (1).

$$2\text{Pt} + 2\text{H}_{ads} \rightarrow 2\text{Pt} + 2\text{H}^+ + 2\text{e}^- \tag{1}$$
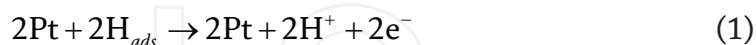
In the case of the Pt_2Mo_8/MWCNTs nanostructure, the high selectivity for HOR is attributed to the interaction between the OH^- group with the oxyphilic metal (Mo) and the Pt nanoparticles that provide active sites for hydrogenation as indicated by the following Eq. (2) [47]:

$$2\text{Pt} + Mo - OH \rightarrow Pt + \text{M} + \text{H}^+ + \text{e}^- \tag{2}$$
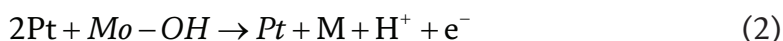
Nakajama and Kita [49] found that the redox couple of Mo^{+2}/Mo^{+3} plays a key role in the enhancement of the catalytic activity of the Pt electrode at low overpotentials. Mo shifts the oxidation of weakly adsorbed OH^- to lower potentials, and therefore, the co-catalytic effect of Pt can set in. The anodic sweep to a greater potential of 0.51 V starts with the adsorption of oxygenated species. The Pt_2Mo_8/MWCNTs nanostructure presents more adsorption of oxygenated species between a potential of 0.51 and 0.66 V. According to the Pourbaix diagram of Mo, at that condition, it forms intermediates mainly oxide species as MoO^{+2}; MoO2; Mo4O11; Mo8O23; Mo9O26; MoO3 and produces a protective oxide film on the metal surface [36]. The adsorption of OH^- and of different oxide species formed on the working electrode surface of the Pt-Mo/MWCNTs nanostructures arises after 0.8 V/NHE. The Pt_5Mo_5/MWCNTs present more adsorption of oxygenated species, from 0.8 to 1.2 V/NHE.

In the cathodic sweep, oxides and their desorption reduction begin approximately at 1.0 V/NHE. All samples reach a maximum current density between 0.71 and 0.63 V/NHE for the ORR. Pt_5Mo_5/MWCNT and Pt_2Mo_8/MWCNTs exhibited a greater oxygen reduction reaction. **Figure 4** confirms this behavior due to the highest intensity in the peak. The oxygen reduction takes place to low potential (0.63 V) by the Pt_2Mo_8/MWCNTs nanostructure. Finally, the capacitive zone is observed in a potential range of 0.35 at 0.45 V, an area without adsorbed or desorbed chemical species. In the case of cyclic voltammogram for the sample Mo_{10}/MWCNTs, it was no observed electrocatalytic activity in the ORR. This is confirmed by the low current density presented and by the absence of peaks in the redox processes at different voltage values. The absence of electroactivity of the Mo/MWCNTs nanostructure is attributed to the high affinity of Mo to oxygenated species (Mo-O bond of 607 bond strength kJ mol^{-1}) [50]. The strong adsorption causes the electrode surface to be saturated with too many layers of oxygenated chemical species inhibiting the reaction [51]. Therefore, it is important to include al Mo in bimetallic or trimetallic alloys in an adequate amount for the ORR.

Figure 5(**a-e**) presents polarization curves obtained by the linear voltammetry technique with different rotation speeds of the different Pt-Mo/MWCNTs nanostructures. Lineal voltammetry of relationships Pt_{10}, Pt_8Mo_2, Pt_5Mo_5, and Pt_2Mo_8 (**Figure 5a-d**) presents a stable behavior in the region I (0.98–0.864 V). In this region, I, the reaction's

speed is controlled by the electronic transfer [52]. Region III is a diffusion zone controlled by mass transport, which is observed at a less positive potential. In this region, there is an influence on the speed of rotation of the electrode. The well-defined horizontal plateaus whose density of current increases as the electrode rotation speed increases indicates a good distribution of active sites and a correct diffusion of oxygen on the surface of the electrode [5, 53]. Region II is a mixed zone, presenting an electronic and mass transference. Linear voltammetry of **Figure 5**(**e**) confirms that the nanostructure
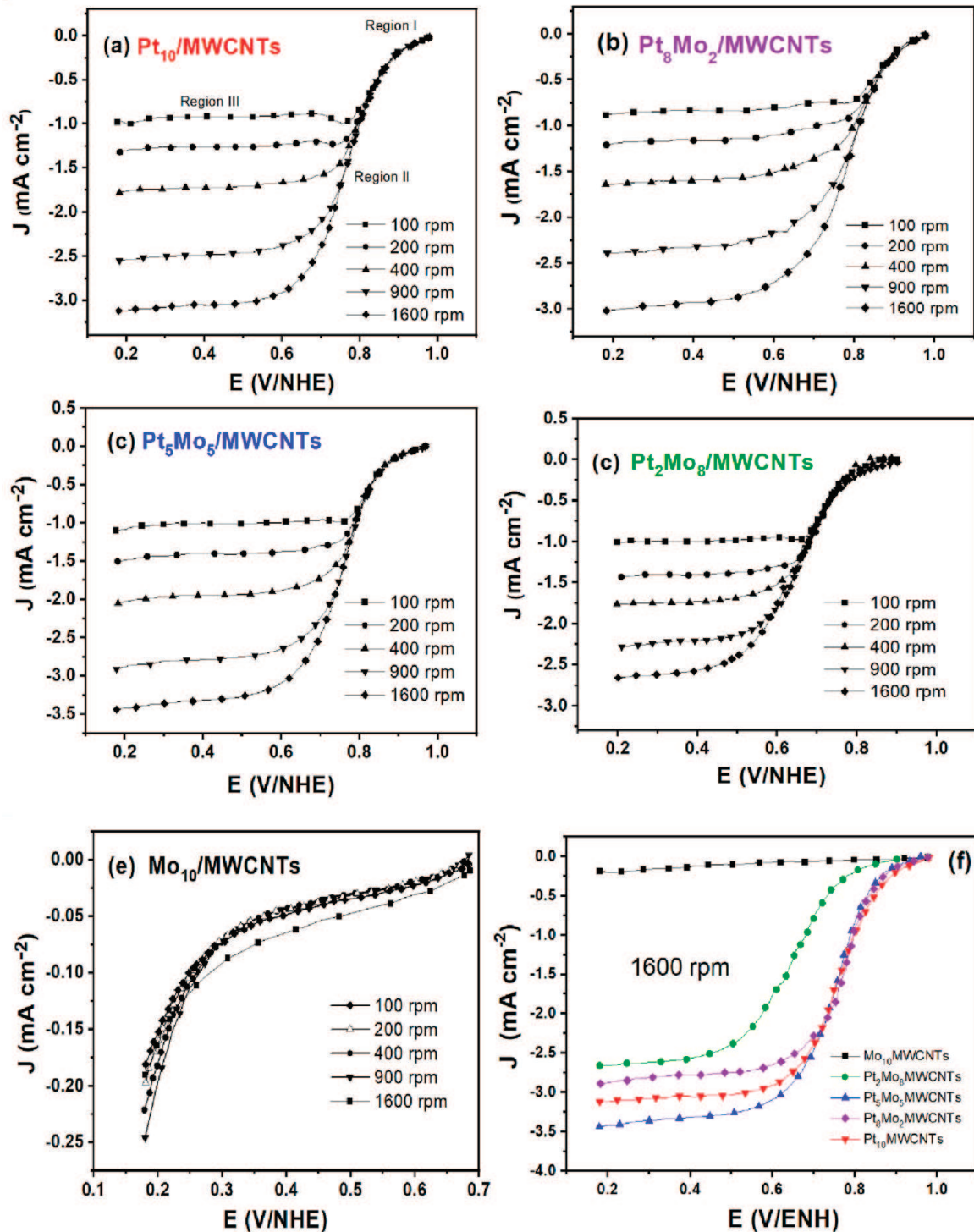

Figure 5.
(a-e). Lineal voltammetry of Pt10/MWCNTs, Pt8Mo2/MWCNTs, Pt5Mo5/MWCNTs, Pt2Mo8/MWCNTs, and Pt10/MWCNTs. (f) Lineal voltammetry comparative at 1600 rpm.

Mo_{10}/MWCNTs does not present electrocatalytic activity in the ORR, because it presents a minimum current density for the different curves. Furthermore, there is an absence of the three control zone characteristics of the ORR. There is no influence by the rotation speed of not presenting the horizontal plateaus that define this type of diffusion. So, in this sample, there is no transfer control of mass.

The electrochemical activity of the five nanostructures is compared through the RDE to 1600 rpm, analysis, see **Figure 5(f)**. The best performance of nanostructures at 1600 rpm, in descending form, is found as follows: $Pt_5Mo_5 > Pt_{10} > Pt_8Mo_2 > Pt_2Mo_8 > Mo_{10}$ with its highest current densities of -3.45, -3.3, -3.2, -2.4, and -0.25 mA cm^2, respectively. The most negative value of the current density is attributed to the smaller particle size of Pt-Mo and a better dispersion on the MWCNT support [54].

Partial slopes of Tafel are depicted in **Figure 6**. The current response is reported in a low range of potential (0.75–0.95 V/NHE), where a linear relation of potential (V) versus log kinetic current density (J_k) is appreciated.

Table 1 summarizes the kinetic parameters for the ORR. Tafel slope values between 60 and 120 mVdec^{-1} showed that ORR catalyzed by Pt-Mo/MWCNTs nanostructures follows a four-electron reduction path to produce water molecules. Representing the well-known reaction of oxygen electro-reduction in an acid solution, it can be written as follows Eq. (3):

$$O_{2ads} + 4H^+ + 4e^- \rightarrow H_2O \qquad (3)$$
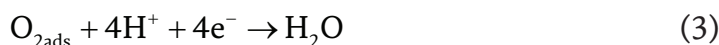
For a fuel cell (PEMFC), the reaction must take place by the previous path since sometimes it can present peroxides as reaction intermediaries that damage the components of the fuel cells device [55]. To quantitatively determine the percentage of peroxide formed should complement the study with other techniques such as the mass spectrophotometer and impedance, which are not within the scope of this work.
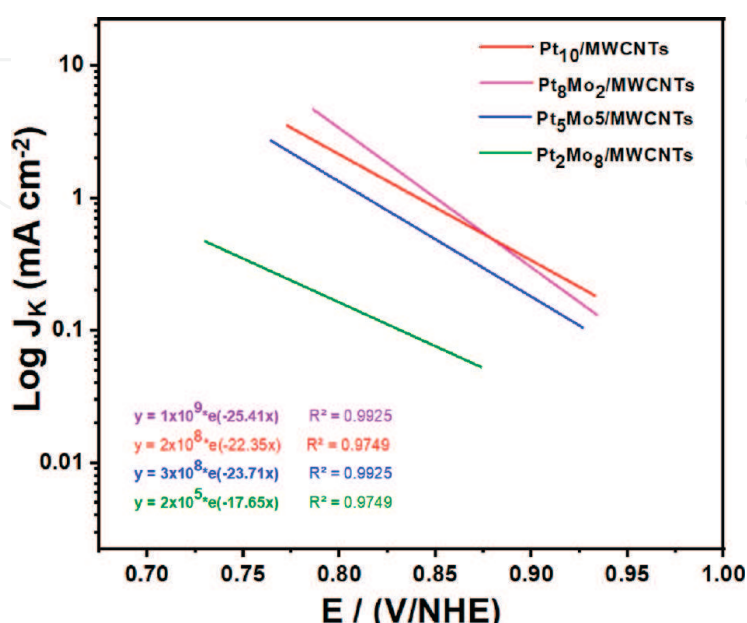
Figure 6.
Partial slopes of Tafel of Pt2Mo8/MWCNTs, Pt5Mo5/MWCNTs, Pt8Mo2/MWCNTs, and Pt10/MWCNTs nanostructures for ORR.

Catalysts	E_{oc} [V/NHE]	b [Vdec^{-1}]	α	j_0 [mAcm-2]	E [V/NHE] to a current of 1 mAcm−2	η overpotential [V/NHE]
Pt10/MWCNTs	0.981	−0.102	0.577	1.23×10^{-4}	0.940	0.249
Pt8Mo2/MWCNTs	0.984	−0.092	0.648	5.58×10^{-5}	0.942	0.246
Pt5Mo5/MWCNTs	0.967	−0.097	0.609	5.70×10^{-5}	0.920	0.263
Pt2Mo8/MWCNTs	0.864	−0.129	0.456	6.87×10^{-5}	0.820	0.336
Mo10/MWCNTs	0.680	—	—	—	—	0.550

Table 2.
Kinetic parameters for the ORR.

When the kinetic parameters are measured for the ORR (**Table 2**), a comparison of the open circuit potential (E_{oc}) with concern to a specific current is obtained. The Pt_8Mo_2/MWCNTs nanostructure presented a potential (0.984 V) closer to the reference potential (1.23 V) with better performance.

In the column of E [V/NHE], the potential is reported to a current density of 1 mA cm^{-2}, confirming that the Pt_8Mo_2/MWCNTs nanostructure is the one that presents the greatest potential that is 0.942 V/NHE. Pt_{10}/MWCNTs nanostructure has similar behavior (0.940 V/NHE). Exchange currents and transfer coefficients are qualitative values and are in the range of platinum catalysts for the ORR [56]. The Pt_8Mo_2/MWCNTs showed a lower slope of Tafel, with a potential value of −0.092 V indicating a mechanism of first order [56, 57]. This means a formation of O_2 directly to the water with a lower potential value (E) of 0.920 V but very close to that obtained with the nanostructure from Pt_5Mo_5/MWCNTs, (−0.097 V) with the advantage of reducing the Pt amount of 50 wt.% in the nanostructure. Additionally, the Pt_8Mo_2/MWCNTs nanostructure has the lowest overpotential concerning 1.23 V required in the oxygen reduction reaction with a value of 0.246 V. The nanostructures of Pt_2Mo_8/MWCNTs and Mo_{10}/MWCNTs require a higher overpotential of 0.354–0.550 V, indicating a different mechanism of four electrons in the ORR.

Mo_{10}/MWCNTs nanostructure could not obtain the kinetic parameters since it does not present electrocatalytic activity toward the ORR. Exchange currents (j_o) and the transference coefficients (α) are qualitative values closing for Pt_5Mo_5/MWCNTs and Pt_{10}/MWCNTs samples. Their catalytic activity is in the range of platinum catalysts for the ORR.

4. Conclusions

Synthesis of Pt-Mo/MWCNTs nanostructures by a green chemical route was presented. The Pt-Mo/MWCNTs with different ratios Pt:Mo were structurally and morphologically characterized, obtaining particle sizes between 3.94 and 10.97 nm by the TEM technique. Particle size and good dispersion are important factors in the performance of an electrocatalytic activity in the ORR. Molybdenum is a reducing

agent (oxyphilic metal) that benefits the adsorption of oxygenated species. The Pt:Mo 8:2 wt.% ratio presents the maximum benefits in the kinetic parameters. The Mo_{10}/MWCNTs nanostructure inhibits the ORR due to the strong bonds it presents with oxygen. Molybdenum at low concentrations with platinum is conducive to the adsorption–desorption of oxygen molecules by increasing the electroactivity in the ORR. Concerning Pt_8Mo_2, it can improve the electrocatalytic activity closer to the response of the catalyst Pt_{10}/MWCNTs with a transference of first order and without inhibition of the reaction. According to the slopes of Tafel obtained in this work for all Pt-Mo/MWCNTs nanostructures, the main stage of the reaction is the transference of the first electron from the electrode to the oxygen molecule adsorbed on the surface of the electrode. The mechanism found is of four electrons for the nanostructures with Pt_{10}, Pt_5Mo_5, Pt_2Mo_8 content; however, for the Pt_8Mo_{10} and Mo_{10} samples, a deeper study will have to be done to determine it.

Acknowledgements

Author details

Esther Torres-Santillan[1]*, Selene Capula-Colindres[2,3], Gerardo Teran[1,3], Carmen M. Reza-San German[1], Miriam Estrada Flores[1] and Oscar Guadalupe Rojas Valencia[1]

1 Departamento de Ingeniería Química, CDMX, México

2 Centro de Investigación en Computación, CDMX, México

3 Departamento de Metalurgia, CDMX, México

*Address all correspondence to: estorress@ipn.mx

IntechOpen

References

[1] Dresselhaus MS, Thomas IL. Alternative energy technologies. Nature. 2001;**414**:332-337. DOI: 10.1038/35104599

[2] Su H, Felix C, Barron O, Bujilo P, Blandergroen B, Pollet B, et al. High-performance and durable membrane electrode assemblies for high-temperature polymer electrolyte membrane fuel cells. Electrocatalysis. 2014;**5**(4):361-371. DOI: 10.1007/s12678-014-0202-5

[3] Kuzume A, Herrero E, Feliu JM. Oxygen reduction on stepped platinum surfaces in acidic media. Journal of Electroanalytical Chemistry. 2007;**599**(2):333-343. DOI: 10.1016/j.jelechem.2006.05.006

[4] Hongchao Y, Yejun Z, Feng H, Qiangbin W. Urchin-like CoP nanocrystals as hydrogen evolution reaction and oxygen reduction reaction dual-electrocatalyst with superior stability. Nano Letters. 2015;**15**(11):7616-7620. DOI: 10.1021/acs.nanolett.5b03446

[5] Pozio A, Giorgi L, Antolini E, Passalacqua E. Electroxidation of H_2 on Pt/C Pt–Ru/C and Pt–Mo/C anodes for polymer electrolyte fuel cell. Electrochimica Acta. 2000;**46**:555-561

[6] Anderson AB, Cai Y, Sidik RA, Kang DB. Advancements in the local reaction center electron transfer theory and the transition state structure in the first step of oxygen reduction over platinum. Journal of Electroanalytical Chemistry. 2005;**580**(1):17-22. DOI: 10.1016/j.jelechem.2005.03.009

[7] Kundu PP, Dutta K. Hydrogen fuel cells for portable applications. In: Compendium of Hydrogen Energy. Vol. 4. Woodhead Publishing (Elsevier); 2016. pp. 111-131

[8] Bing Y, Liu H, Zhang L. Nanostructured Pt-alloy electrocatalysts for PEM fuel cell oxygen reduction reaction. Chemical Society Reviews. 2010;**39**(6):2184-2202

[9] Wang H, Macomber C, Christ J, Benser G, Pivovar B, Dinh HN. Evaluating the influence of PEMFC system contaminants on the performance of Pt catalyst via cyclic voltammetry. Electrocatalysis. 2014;**5**(1):62-67. DOI: 10.1007/s12678-013-0159-9

[10] Mao L, Jackson L, Davies B. Investigation of PEMFC fault diagnosis with consideration of sensor reliability. International Journal of Hydrogen Energy. 2018;**43**(35):16941-16948. DOI: 10.1016/j.ijhydene.2017.11.144

[11] Park IS, Tong YYJ. Sulfide-Adsorption enhanced oxygen reduction reaction on carbon-supported Pt electrocatalyst. Electrocatalysis. 2013;**4**(3):117-122. DOI: 10.1007/s12678-013-0132-7

[12] Fernandes AC, Paganin VA, Ticianelli EA. Degradation study of Pt-based alloy catalysts for the oxygen reduction reaction in proton exchange membrane fuel cells. Journal of Electroanalytical Chemistry. 2010;**648**:156-162. DOI: 10.1016/j.jelechem.2010.07.013

[13] Shao M, Chang Q, Dodelet J-P, Chenitz R. Recent advances in electrocatalysts for oxygen reduction reaction. Chemical Reviews. 2016;**16**:3594-3657. DOI: 10.1021/acs.chemrev.5b00462

[14] Sharma S, Pollet BG. Support materials for PEMFC and DMFC electrocatalysts—A review. Journal of Power Sources. 2012;**208**:96-119

[15] Dong Y, Xue Y, Gu W, Yang Z, Xu G. MnO_2 nanowires/CNTs composites as efficient non-precious metal catalyst for oxygen reduction reaction. Journal of Electroanalytical Chemistry. 2019;**837**(15):55-59. DOI: 10.1016/j.jelechem.2019.02.012

[16] Delmondo L, Salvador GP, Muñoz JA, Sacco A, Garino N, Castellino M, et al. Nanostructured MnxOy for oxygen reduction reaction (ORR) catalysts. Applied Surface Science. 2016;**338**(B):631-639. DOI: 10.1016/j.apsusc.2016.03.224

[17] Yufei M, Guoqing G, Xiaogang H, Ji C, Abuliti A. Molybdenum carbide as alternative catalyst for hydrogen production – A review. Advanced Materials Research. 2017;**75**:1101-1129. DOI: 10.1016/j.rser.2016.11.092

[18] Zhang X, Shi C, Chen B, Kuhn AN, Ma D, Yang H. Progress in hydrogen production over transition metal carbide catalysts: Challenges and opportunities. Current Opinion in Chemical Engineering. 2018;**20**:68-77. DOI: 10.1016/j.coche.2018.02.010

[19] Liu J, Sun CQ, Zhu W. Origin of efficient oxygen reduction reaction on Pd monolayer supported on Pd-M (M= Ni, Fe) intermetallic alloy. Electrochimica Acta. 2018;**282**(20):680-886. DOI: 10.1016/j.electacta.2018.06.041

[20] Shao M, Yu T, Odell JH, Xia Y. Structural dependence of oxygen reduction reaction on palladium nanocrystals. Chemical Communications. 2011;**47**(23):6566-6568

[21] Nekooi P, Amini MK. Effect of support type and synthesis conditions on the oxygen reduction activity of RuxSey catalyst prepared by the microwave polyol method. Electrochimica Acta. 2010;**55**(9):3286-3294. DOI: 10.1016/j.electacta.2009.12.102

[22] Patel PR, Kuruba R, Damodaran K, Jampani P, Gattu B, Shanthi PM, et al. Noble metal-free bifunctional oxygen evolution and oxygen reduction acidic media electro-catalysts. Scientific Reports. 2016;**6**(28367):1-14. DOI: 10.1038/srep28367

[23] Luo J, Yin J, Loukrakpam R, Wanjala BN, Fang B, Shan S, et al. Design and electrochemical characterization of ternary alloy electrocatalysts for oxygen reduction reaction. Journal of Electroanalytical Chemistry. 2013;**688**:196-206. DOI: 10.1016/j.jelechem.2012.09.032

[24] Zagal JH. Handbook of Fuel Cells - Fundamentals Technology and Applications2003. pp. 545-554

[25] Nguyet NAT, Shim JH. Facile one-step synthesis of Ir-Pd bimetallic alloy networks as efficient bifunctional catalysts for oxygen reduction and oxygen evolution reactions. Journal of Electroanalytical Chemistry. 2018;**827**(15):120-127. DOI: 10.1016/j.jelechem.2018.09.012

[26] Jahan M, Bao Q, Yang JX, Loh KP. Electrocatalytically active graphene–porphyrin MOF composite for oxygen reduction reaction. Journal of the American Chemical Society. 2012;**134**(15):6707-6713. DOI: 10.1021/ja211433h

[27] Mpeta LS, Nyokong T. Electrocatalytic activity of ethynylbenzyl phthalocyanines when linked to quantum dots via click chemistry: Towards efficient oxygen reduction reaction and H_2O_2 oxidation. Journal

of Electroanalytical Chemistry. 2019;**840**:218-229. DOI: 10.1016/j. jelechem.2019.03.064

[28] Zhang K, Feng C, He B, Dong H, Zhang X. An advanced electrocatalyst of Pt decorated SnO_2/C nanofibers for oxygen reduction reaction. Journal of Electroanalytical Chemistry. 2016;**781**:198-203

[29] Lebedeva NP, Janssen GJM. On the preparation and stability of bimetallic PtMo/C anodes for proton-exchange membrane fuel cells. Electrochimica Acta. 2005;**51**(1):29-40. DOI: 10.1016/j. electacta.2005.04.034

[30] Lee CH, Jun B, Lee SU. Metal-free oxygen evolution and oxygen reduction reaction bifunctional electrocatalyst in alkaline media: From mechanisms to structure–catalytic activity relationship. ACS Sustainable Chemistry & Engineering. 2018;**6**(4):4973-4980

[31] Nepel TCM, Lopes PP, Paganin VA, Ticianelli EA. CO tolerance of proton exchange membrane fuel cells with Pt/C and PtMo/C anodes operating at high temperatures: A mass spectrometry investigation. Electrochimica Acta. 2013;**88**:217-224. DOI: 10.1016/j. electacta.2012.10.039

[32] Mukerjee S, Lee SJ, Ticianelli EA, McBreen J, Grgur BN, Markovic NM, et al. Investigation of enhanced CO tolerance in proton exchange membrane fuel cells by carbon supported PtMo alloy catalyst. Electrochemical and Solid-State Letters. 1999;**2**(1):12-15

[33] Puello PE, Ayala M, Brito JBL. Activated carbon supported cobalt-molybdenum carbides: effect of the synthesis method, heating rate, type of cobalt precursor and presulfiding agent on thiophene hydrodesulfurization. Revista Facultad de Ingeniería. 2014;**70**:75-85

[34] Dai Y, Sun K, Li Y. Mo-Pt core–shell nanoparticles as an efficient electrocatalyst for oxygen reduction reaction. Journal of Electroanalytical Chemistry. 2015;**757**:94-99. DOI: 10.1016/j.jelechem.2015.09.020

[35] Pérez- González A, Gómez-Peralta JI, Garza-Ortiz A, Barba-Behrens N. The relevance of molybdenum in biological systems and its role in the mononuclear enzymes with the *Moco* cofactor. Educación química. 2012;**23**(1):24-33

[36] Nikolaychuk PA, Tyurin AG. The revised Pourbaix diagram for molybdenum. Butlerov Communications. 2011;24(2):101-105. Available from: http://butlerov.com/files/reports/2011/vol24/2/101/101-105.pdf

[37] Iwamoto M, Yoda Y, Yamazoe N, Seiyama T. Study of metal oxide catalysts by temperature programmed desorption. 4. Oxygen adsorption on various metal oxides. The Journal of Physical Chemistry. 1978;**82**(24):2564-2570. DOI: 10.1021/j100513a006

[38] Hussain S, Erikson H, Kongi N, Merisalu M, Ritslaid P, Sammelselg V, et al. Heat-treatment effects on the ORR activity of Pt nanoparticles deposited on multi-walled carbon nanotubes using magnetron sputtering technique. International Journal of Hydrogen Energy. 2017;**42**(9):5958-5970

[39] Huang B, Peng L, Yang F, Liu Y, Xie Z. Improving ORR activity of carbon nanotubes by hydrothermal carbon deposition method. Journal of Energy Chemistry. 2017;**26**:712-718. DOI: 10.1016/j.jechem.2017.03.016

[40] Fang B, Pinaud BA, Wilkinson DP. Carbon-supported Pt hollow nanospheres as a highly efficient electrocatalyst for the oxygen reduction reaction. Electrocatalysis.

2016;**7**(4):336-344. DOI: 10.1007/s12678-016-0311-4

[41] Luais E, Mery A, Abou-Rjeily J, Sakai J. A self-standing and binder-free electrodes fabricated from carbon nanotubes and an electrodeposited current collector applied in lithium-ion batteries. Journal of Electrochemical Science and Technology. 2019;**10**(4):373-380. DOI: 10.33961/jecst.2019.03132

[42] Alhamoud Y, Yang D, Kenston SSF, Liu G, Liu L, Zhou H, et al. Advances in biosensors for the detection of ochratoxin A: Bio-receptors, nanomaterials, and their applications. Biosensors and Bioelectronics. 2019;**141**:11418. DOI: 10.1016/j.bios.2019.111418

[43] Torres-Santillan E, Capula S, Reza CM, Cayetano NC, Villagarcia EC. Effect of functional groups in the structure of carbon nanotubes to adsorption grade of cadmium ions. Revista Mexicana de Ingenieria Quimica. 2018;**17**(3):955-961. DOI: 10.24275/uam/izt/dcbi/revmexingquim/2018v17n3/Torres

[44] Gao J, Zou J, Zeng X, Ding W. Carbon supported nano Pt–Mo alloy catalysts for oxygen reduction in magnesium–air batteries. RSC Advances. 2016;**6**:83025-83030. DOI: 10.1039/C6RA16142A

[45] Del Colle V, Perroni PB, Feliu JM, Tremiliosi-Filho G, Varela H. The role of surface sites on the oscillatory oxidation of methanol on stepped Pt[n(111)×(110)] electrodes. Journal of Physical Chemistry C. 2020;**124**(20):10993-10004. DOI: 10.1021/acs.jpcc.0c01897

[46] Zhao Y, Fan L, Ren J, Hong B. Electrodeposition of Pt–Ru and Pt–Ru–Ni nanoclusters on multi-walled carbon nanotubes for direct methanol fuel cell. International Journal of Hydrogen Energy. 2014;**39**(9):4544-4557. DOI: 10.1016/j.ijhydene.2013.12.202

[47] Capula SC, Aguir K, Cervantes FS, Villa LV, Moncayo JS, Garibay VF. Ozone sensing based on palladium decorated carbon nanotubes. Sensor. 2014;**14**:6806-6818

[48] Grgur BN, Markovy NM, Ross PN. Electrooxidation of H2, CO and H_2/CO mixtures on well characterized PtMo alloy. Journal of the Serbian Chemical Society. 2003;**68**(3):191-205

[49] Nakajima H, Kita H. The role of surface molybdenum species in methanol oxidation on the platinum electrode. Electrochimica Acta. 1990;**35**(5):849-853

[50] Robinson M, Montemore MM, Tenney SA, Sutter P, Medlin JW. Interactions of hydrogen, CO, oxygen, and water with molybdenum-modified Pt(111). Journal of Physical Chemistry C. 2013;**117**(50):26716-26724. Available from: https://pubs.acs.org/doi/10.1021/jp410563s

[51] Robinson AM, Hensley JE, Medlin JW. Surface chemistry of aromatic reactants on Pt- and Mo-modified Pt Catalysts. Journal of Physical Chemistry C. 2016;**120**(47):26824-26833. DOI: 10.1021/acs.jpcc.6b08415

[52] Torres-Santillan E, Vargas-Garcia JR, Ramirez-Meneses E, Manzo-Robledo A, Hernandez-Perez MA. Induced electrochemical reduction of nitrates species on interface of Pt/MWCNTs prepared by vapor-phase impregnation-decomposition method. Revista Mexicana de Ingenieria Quimica. 2019;**18**(2):431-443. DOI: 10.24275/uam/izt/dcbi/revmexingquim/2019v18n2/Torres

[53] Antolini E. Formation of carbon-cupported PtM alloys for low temperature fuel cells. Materials

Chemistry and Physics. 2003;**28**:563-573.
DOI: 10.1016/S0254-0584(02)00389-9

[54] Rossmeisl J, Qu Z-W, Zhu H, Kroes G-J, Nørskov JK. Electrolysis of water on oxide surfaces. Journal of Electroanalytical Chemistry. 2007;**607**(1-2):83-89. DOI: 10.1016/j.jelechem.2006.11.008

[55] Morante-Catacora TY, Ishikawa Y, Carlos R. Cabrera Sequential electrodeposition of Mo at Pt and PtRu methanol oxidation catalyst, particles on HOPG surfaces. Journal of Electroanalytical Chemistry. 2008;**621**:103-112. DOI: 10.1016/j.jelechem.2008.04.029

[56] Zhang J, Cui R, Li X, Liu X, Huang W. A nanohybrid consisting of NiPS3 nanoparticles coupled with defective graphene as a pH-universal electrocatalyst for efficient hydrogen evolution. Journal of Materials Chemistry A. 2017;**5**(45):23536-23542. DOI: 10.1039/c7ta07672j

[57] Cui Y, Zhou C, Li X, Gao Y, Zhang J. High-performance electrocatalysis for hydrogen evolution reaction using nickel-doped CoS2 nanostructures: Experimental and DFT insights. Electrochimica Acta. 2017;**228**:428-435. DOI: 10.1016/j.electacta.2017.01.103